


 Cite this: *RSC Adv.*, 2023, 13, 9824

Density functional theory computation of the intermolecular interactions of $\text{Al}_2\text{@C}_{24}$ and $\text{Al}_2\text{@Mg}_{12}\text{O}_{12}$ semiconducting quantum dots conjugated with the glycine tripeptide

 Hadi Mohammadi,^a S. M. Azami^b and Hashem Rafii-Tabar^{*,ac}

The nature of intermolecular forces within semiconductor quantum dot systems can determine various physicochemical properties, as well as their functions, in nanomedical applications. The purpose of this study has been to investigate the nature of the intermolecular forces operating between $\text{Al}_2\text{@C}_{24}$ and $\text{Al}_2\text{@Mg}_{12}\text{O}_{12}$ semiconducting quantum dots and the glycine tripeptide (GlyGlyGly), and also consider whether permanent electric dipole–dipole interactions play a significant role *vis-à-vis* these molecular systems. The energy computations, including the Keesom and the total electronic interactions and the energy decomposition, together with the quantum topology analyses were performed. Our results demonstrate that no significant correlation is found between the magnitude and orientation of the electrical dipole moments, and the interaction energy of the $\text{Al}_2\text{@C}_{24}$ and $\text{Al}_2\text{@Mg}_{12}\text{O}_{12}$ with GlyGlyGly tripeptide. The Pearson correlation coefficient test revealed a very weak correlation between the quantum and the Keesom interaction energies. Apart from the quantum topology analyses, the energy decomposition consideration confirmed that the dominant share of the interaction energies was associated with the electrostatic interactions, yet both the steric and the quantum effects also made appreciable contributions. We conclude that, beside the electrical dipole–dipole interactions, other prominent intermolecular forces, such as the polarization attraction, the hydrogen bond, and the van der Waals interactions can also influence the interaction energy of the system. The findings of this study can be utilized in several areas in the field of nanobiomedicine, including the rational design of cell-penetrating and intracellular drug delivery systems using semiconducting quantum dots functionalized with a peptide.

 Received 20th February 2023
 Accepted 21st March 2023

DOI: 10.1039/d3ra01154b

rsc.li/rsc-advances

1. Introduction

Intermolecular forces of semiconducting quantum dots (SCQDs) play a decisive role in diverse fields ranging from nanoscopic self-assembly¹ to various nanofabrication processes, based on inter-particle forces,^{2–5} and supramolecular assembly of macromolecules as in bio-molecular recognition applications.^{6–9} They play a significant role in accounting for both structure-stability and structure–function in the above-mentioned fields. For instance, long-range electrostatic effects, either attractive or repulsive,¹⁰ perform a crucial role in related biological phenomena^{11,12} such as in the protein function¹³ and in the DNA repair process¹⁴ as well as DNA deformation.¹⁵ These intermolecular forces modulate the active sites

of some enzymes.¹⁶ Similarly, they play a decisive role in the field of pharmacology, ranging from drug discovery to the investigation of drug-receptor coupling.^{17–21} The majority of scientists have paid a great deal of attention to the consequences of these classical intermolecular interactions.^{7,8,11,12,17–19,22,23}

From the perspective of cellular level, several research groups have carried out their study with reference to the field of nanomedicine, specifically the interactions of nanostructures, or quantum dots, with cells, biomolecules, and proteins.^{24–30} For instance, Forest *et al.*³¹ have pointed out the significant role of electrostatic interactions in relation to nano-bio systems, which consist of the interactions of cells with nanoparticles that are coupled to them *via* the surface of the cell membranes. Furthermore, Nel *et al.*³² have considered the biophysical interactions at the interface of nano-bio systems. Consequently, they have demonstrated that the nature of these biophysical interactions is the same as those between some colloidal particles that interact *via* electrostatic, hydrophobic, van der Waals(vdW), solvophobic, solvation interactions, as well as the

^aDepartment of Medical Physics and Biomedical Engineering, School of Medicine, Shahid Beheshti University of Medical Sciences, Tehran, Iran. E-mail: rafii-tabar@nano.ipm.ac.ir

^bDepartment of Chemistry, Faculty of Sciences, Yasouj University, Yasouj, Iran

^cThe Physics Branch of the Academy of Sciences of Iran, Tehran, Iran



depletion forces.³² Consequently, the majority of studies have indicated that specific intermolecular forces, such as those mentioned above, compared with nonspecific forces, such as the hydrophobic one, play a vital role *vis-à-vis* the cellular uptake of nanoparticles at the nano-bio interfaces.³³

In addition to the cellular level, the electrostatic forces at the molecular level are defined by several types of interactions, *i.e.*, the charge–charge, the charge–dipole and the permanent dipole–permanent dipole interactions, that are important in gas or liquid or solvent phases.³⁴ Therefore, the electrical dipole–dipole interactions are categorized as electrostatic in nature, and they are more effective in connection with the interactions of nanostructures with biomolecules.^{35–37} As an example, Vovusha *et al.* have employed the density functional theory (DFT) to investigate the mutual interactions between the permanent electrical-dipole-moment orientations of the h-BN/graphene nanoflake with nucleobases. Their results indicate that not only the special orientation of the hybrid nanoflake in relation to nucleobases has a significant role in stabilizing the system, but also the most accessible configurations of the h-BN/graphene nanoflake with nucleobases were found to be the antiparallel orientation.³⁸ Similarly, in the field of medicinal chemistry and drug design, the electrical dipole moment plays an important role as a descriptor in the quantitative-structure–activity-relationship (QSAR) in order to discover the biological activity of either the natural products or the synthetic compounds.^{39,40} For instance, Riahi and coworkers⁴¹ have computed the effect of Efavirenz drug (as a potentially anti-cancer drug) on DNA to reveal the nature of the intermolecular interaction between them. Their results showed that the appropriate interaction is composed of the electrostatic and dispersion forces at the drug–nucleobase interface leading to the stability of the complexes.

Summarizing the above-mentioned points, we can regard the electrical dipole–dipole intermolecular forces as playing a significant role either at the nano-bio interfaces or in pharma systems. Furthermore, the classical electrostatic interactions have been considered more extensively compared with the quantum effects.

Therefore, the aim of our paper has been to systematically explore the origin of the intermolecular forces through a molecular model *via* the DFT calculations, and ascertain whether or not the electrical dipole–dipole interactions always play a decisive role in the stability of the selected molecular systems at the nano-bio interfaces including intercellular drug delivery design based on peptides as a target vector. When employing the quantum mechanical approach to study the nano-bio systems, we need to select an approach within this methodology which provides an adequate level of information by using a rather reasonable amount of computational time, and cost. Consequently, both the configuration interaction (CI)^{42,43} approach and the Møller–Plesset perturbation theory (MPn)⁴⁴ are considered as higher wave function-based quantum mechanical approaches, compared with the Hartree–Fock (HF) approaches, which take into account the electron–electron correlation, but with a higher computational costs that could form a significant limitation for their use. Therefore, the

rationale behind using the DFT method is associated with its exceptional level of accuracy with reduced computational time and being cost effective in comparison to the above-mentioned methods.

To the best of our knowledge, this is the first time that these two particular SCQDs, that have wide-ranging applications in biomedical fields,^{45–49} have been investigated. To implement this objective two sets of organic and inorganic SCQDs, including Al₂@C₂₄ and Al₂@Mg₁₂O₁₂, interacting with (conjugated with) the GlyGlyGly tripeptide, are considered in order to carry out qualitative and quantitative analyses. Our results ascertain that in addition to the electrical dipole–dipole interactions, the intermolecular forces, such as the polarization attraction, the hydrogen bonding and the vdW interactions play a rather significant role in nanobiomedical systems, and that the intermolecular forces in these systems are not ignorable, *vis-à-vis* the stability, nor are they ignorable in relation to the properties of the molecular systems themselves.

The organization of this paper is as follows: in Section 2, we consider the theoretical and computational modeling that has been used to compute the dipole moments of the two quantum dots that have been considered. In Section 3, the results of our computations and their discussion are provided. Section 4 is the concluding part of the paper.

2. Theoretical and computational methods

The Gaussian 16 software package⁵⁰ and the Gauss View 6.1.1 version⁵¹ were employed to carry out all the relevant quantum-mechanical calculations and the corresponding visualization of all the structures that were considered. Furthermore, the ground-state calculations of the specific quantum dots, Al₂@C₂₄ and Al₂@Mg₁₂O₁₂, and the GlyGlyGly tripeptide in the implicit solvent phase model were performed (Fig. 1a–c). The solvent model is represented by the conductor-like polarizable continuum model (CPCM) as well as by the self-consistent reaction field (SCRF).^{52,53} The calculations were optimized at M062X level of the DFT theory using the 6-31++G** basis set. The M062X function is a reliable method since it considers the dispersion long range interactions; it is therefore applied for studying the noncovalent interactions of various nanocages–pharma interfaces.^{54–60} In order to ascertain whether the structures are the optimized ones, frequency computations were performed to probe the nature of the stationary points of the structures.

Our modeling consists of two parts. In the first part, the dipole moments of Al₂@C₂₄, Al₂@Mg₁₂O₁₂, and GlyGlyGly under both optimized and fragmented conditions, and Al₂@C₂₄–GlyGlyGly, and Al₂@Mg₁₂O₁₂–GlyGlyGly complexes under optimized conditions were computed. Furthermore the difference of the two dipole moments representing the ($P_{\text{comp}} - P_{\text{sumopt}}$) and the ($P_{\text{comp}} - P_{\text{sumfrag}}$) states were calculated. Initially the optimized states of Al₂@C₂₄–GlyGlyGly complexes as well as Al₂@Mg₁₂O₁₂–GlyGlyGly systems were guessed with respect to both the orientation and magnitude of the dipole



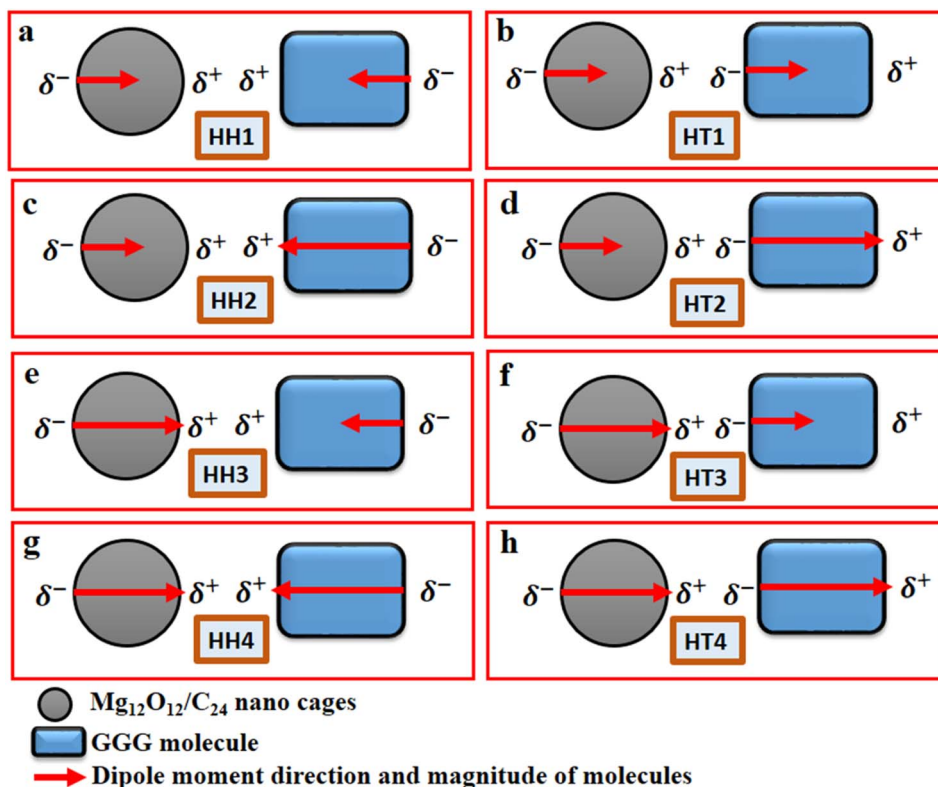


Fig. 1 Schematic representations of two sets of eight molecules, including 1a, 1b, 1g and 1h cases, with the dipole moments referring to the SCQDs and/or GlyGlyGly tripeptide when their dipole moments are either both minimum or maximum; while 1c, 1d, 1e and 1f cases represent the dipole moments when one is minimum and the other one is maximum.

moments. For these calculations, as can be seen in Fig. 1, two sets of eight molecules are considered. In this way, the set of complexes consisting of vertically parallel and horizontally opposed directions of the dipole moments, such as the head-to-tail (HT) and the head-to-head (HH) horizontal orientations could be considered. We considered only the horizontal orientations. As far as the magnitude of the dipole moments of the SCQDs and tripeptide are concerned, according to Fig. 1 we have four HH/HT configurations, denoted by 1 to 4, wherein the numbers 1 and 4 pertain to the cases when the dipole moments are either both minimum or both maximum (as shown in Fig. 1a, b, g and h) and configuration numbers 2 and 3 pertain to the cases when one dipole moment is minimum and the other one is maximum (as shown in Fig. 1c–f). In addition to the dipole moments, two energy calculations are performed; one is the total electronic (TE) energy that represents the quantum interaction energy, and the other is the Keesom energy. At the end of this part, Pearson's regression coefficient was computed as a statistical index, *via* the Origin Pro 2021 software, in order to determine whether there is any correlation between the pertinent variables.

The Keesom (KE) energy is given by.¹⁰

$$KE = -P_1 P_2 [2 \cos \theta_1 \cos \theta_2 - \sin \theta_1 \sin \theta_2 \cos \varphi] / 4\pi \epsilon_0 d^3 \quad (1)$$

where P_1 and P_2 are the electrical dipole moments of the SCQDs and tripeptide respectively, θ_1 and θ_2 are the fixed angles

between the dipole moments P_1 and P_2 and the horizontal axis, and φ is the azimuthal angle of the P_2 dipole moment, d represents the distance between the dipole moments, ϵ_0 is the permittivity of the vacuum.

The second part of our computations was concerned with the analyses of the electronic structures namely; the energy decomposition analysis (EDA), the quantum theory of atoms in molecules (QTAIM), the electron localized function (ELF), the localized orbital locator (LOL), the noncovalent interaction (NCI), and the reduced density gradient (RDG) for the eight selected complexes. These analyses were performed in order to obtain an explicit information concerning the nature of the interactions within the complexes.

Here we briefly state the theoretical basis of the EDA, QTAIM, ELF, LOL, NCI and RDG. The EDA is performed by employing the Shubin Liu (SBL) method.⁶¹ In this method, the interaction energy of the complexes can be decomposed into the electrostatic, steric and quantum terms as expressed by

$$E = E_{el} + E_s + E_q \quad (2)$$

with

$$\begin{aligned} E_{el} &= V_J + V_{nn} + V_{ne} \\ &= \iint \frac{\rho(r_1)\rho(r_2)}{r_{12}} dr_1 dr_2 + \sum_{A>B} \frac{Z_A Z_B}{R_{AB}} - \int \rho(r) \sum_A \frac{Z_A}{|r - R_A|} dr \end{aligned} \quad (3)$$



$$E_s = T_W = |\nabla\rho(r)|^2/[8\rho(r)] \quad (4)$$

$$E_q = E_{\text{pauli}} + E_{\text{XC}} \quad (5)$$

and where E_{el} , E_s and E_q represent independent physicochemical energy contributions from electrostatic, steric and quantum (specifically fermionic quantum) effects respectively. Consequently, as can be observed from eqn (3) the inter-electron Coulomb repulsion (V_j), the nuclear–nuclear repulsion (V_{nn}) and the nuclear–electron attraction (V_{ne}) together constitute the classical terms of the electrostatic energy. In addition, as one can see from eqn (4), E_s has a simple association with the Weizsäcker kinetic energy (TW).⁶¹ Eqn (5) represents the quantum energy effect, composed of the Pauli kinetic energy and the exchange–correlation energy.

The QTAIM, and both the ELF and the LOL, are the complementary electronic structure analyses used for investigating the nature of intermolecular force(s) between GlyGlyGly tripeptide and $\text{Al}_2@C_{24}/\text{Al}_2@Mg_{12}O_{12}$ SCQDs *via* the AIM 2000 software⁶² and the MWfn 3.8 software.⁶³ The QTAIM method is based on Bader's theory⁶⁴ and provides the electronic distribution features and the topological parameters of the selected SCQDs.

The NCI indices, as represented by eqn (6), depend on both the electron density (q) and the RDG,⁶⁵ denoted by s , where s is given by eqn (6). The NCI is computed by using the interactive MWfn 3.8 software⁶³ in order to determine the types of weak interactions among the complexes. The second largest Hessian matrix of eigenvalues (λ_2) of q *versus* the RDG scatter plots obtained by the Multiwfn 3.8 software provides the noncovalent interactions within the complexes. The RDG isosurfaces and the maps of the scatter points are visualized and/or are plotted using the visual molecular dynamics (VMD1.9.4) package,⁶⁶ and the gnu-plot software 5.7⁶⁷ respectively.

$$s(r) = \frac{1}{2(3\pi^2)^{1/3}} \frac{|\nabla\rho(r)|}{\rho(r)^{4/3}} \quad (6)$$

where $\rho(r)$ is the electron density and $\nabla\rho(r)$ is the density gradient at bond critical points (BCPs).

3. Results and discussion

3.1. Calculation of various dipole moments

Fig. 2 displays the selection of some of the optimized structures under the isolated (Fig. 2a–c), and the complexes conditions (Fig. 2d and e) for both SCQDs and the GlyGlyGly biomolecule together with the orientations of their corresponding dipole moments. Here, we have solely taken into account the horizontally opposite states, including the HH as well as the HT directions, of the individual dipole moments as the initial conditions for the computations. Furthermore, we have applied geometry optimization not only for obtaining the possible ground state of the molecules, but also to extract the orientation and magnitude of the dipole moments for the SCQDs and GlyGlyGly. The optimization of the molecules was performed under different situations namely; the isolated, the combined,

i.e., SCQDs and GlyGlyGly, and the frozen fragment conditions in which the Cartesian coordinates are fixed, whereas they change in the complex. Both the frozen fragment conditions and the complexes conditions are used to calculate the binding energy.

Fig. 3 displays the minimum and maximum dipole moments of $\text{Al}_2@C_{24}$ and $\text{Al}_2@Mg_{12}O_{12}$ together with their conjugation with the GlyGlyGly under the optimized conditions. The calculated values of the dipole moments of these molecules were; 0.76 and 30.57 for $\text{Al}_2@C_{24}$ -GlyGlyGly complexes, 4.43 and 50.44 for $\text{Al}_2@Mg_{12}O_{12}$ -GlyGlyGly complexes, 4.7 and 11.12 for $\text{Al}_2@C_{24}$ SCQDs, 0.09 and 34.70 for $\text{Al}_2@Mg_{12}O_{12}$ SCQDs, 4.01 and 14.13 for GlyGlyGly tripeptides, all in the Debye (D) unit. Similarly, the pair of minimum and maximum values of the dipole moments for the frozen fragments of $\text{Al}_2@C_{24}$ and $\text{Al}_2@Mg_{12}O_{12}$ SCQDs were obtained to be (5.00D, 10.64D), (4.04D, 50.34D) respectively. Therefore, it can be seen from the Fig. 3 that for both SCQD-GlyGlyGly complexes, the HT₄ has the highest value, while the HH₁ and the HT₁ have the lowest values for these complexes. Likewise, for the frozen fragment condition, the highest and lowest values were the same as those under the optimized situation.

It should be pointed out that if the dipole–dipole interactions are dominant in the reagent interaction energy within the total electronic energy of the system, then we expect that all the HT configurations to have a higher value of the dipole moments compared to the HH configurations.³⁴ As Fig. 3 shows only the HH₁ and the HT₄, which belong to $\text{Al}_2@C_{24}$ -GlyGlyGly, appear at correct places at the beginning and the end of the graph, while the orders of the other configurations do not correspond to the locations that they should occupy on the graph. Similarly, for $\text{Al}_2@Mg_{12}O_{12}$ -GlyGlyGly cases, the HT₄ and the HT₃ have the highest values of the dipole moments, but instead of the HH₁ configuration appearing on the minimum side of the graph, the HT₁ is seen to be located on the minimum side, which is not its appropriate location.

Fig. 4 represents the difference between the dipole moments of the complete $\text{Al}_2@C_{24}$ -GlyGlyGly complexes (P_{comp}) and the sum of the dipole moments of their constituent parts (P_{sumopt}) under the optimized situation, and the difference between the complete dipole moments of $\text{Al}_2@C_{24}$ -GlyGlyGly complexes and the sum of the dipole moments of their constituent parts under the frozen fragment condition (P_{sumfrag}). The figure also shows the same differences for $\text{Al}_2@Mg_{12}O_{12}$ -GlyGlyGly complexes.

As can be seen from this figure, all of the cases of $\text{Al}_2@C_{24}$ -GlyGlyGly in the segment of head-to-head directions are subtractive except the HH₂ complex, whereas for half of the cases (HT₃ and HT₄), in the head-to-tail sector, they appear to be additive. However, in case of $\text{Al}_2@Mg_{12}O_{12}$ -GlyGlyGly complexes, half of the cases are computed to be either subtractive or additive in both configurations. By “additive” and “subtractive”, we mean when two dipole moments are added together, and when they are subtracted from each other. It should be noted that when two charges, either with the same sign or the opposite sign, interact with each other, the results would appear as either subtractive or additive respectively. Therefore, we observe that for both the HH and the HT



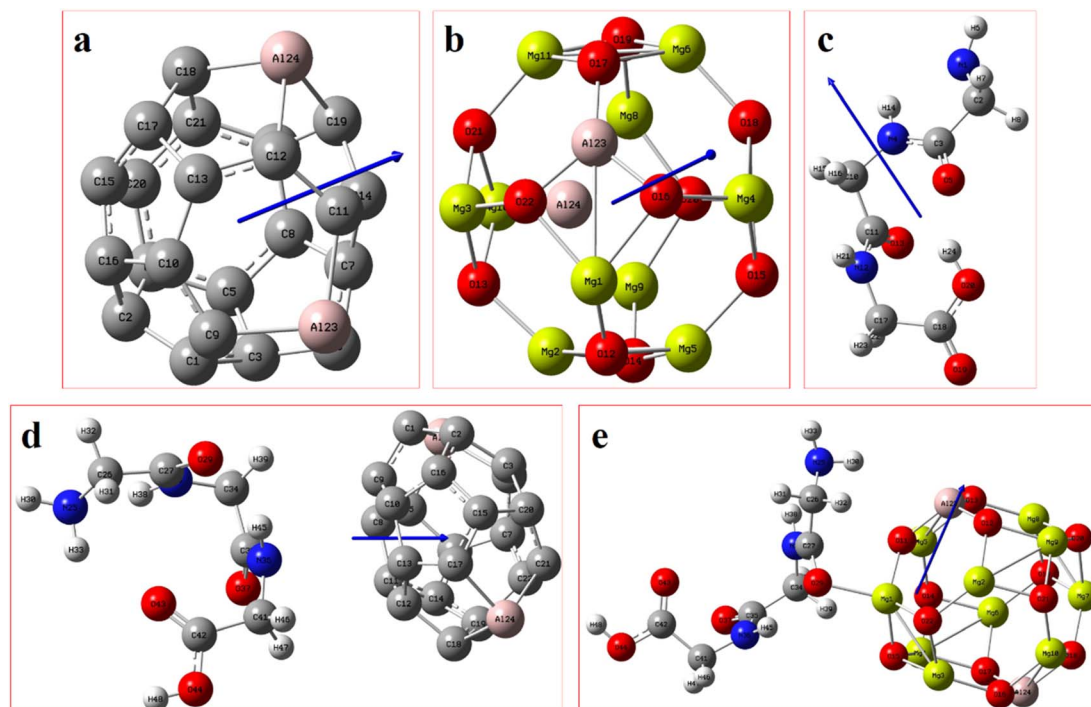


Fig. 2 From the left to right, the blue arrows show the values and directions of the calculated electrical dipole moments of (a) $\text{Al}_2@C_{24}$, (b) $\text{Al}_2@Mg_{12}O_{12}$ SCQDs, and (c) GlyGlyGly tripeptide, (d) $\text{Al}_2@C_{24}$ -GlyGlyGly and (e) $\text{Al}_2@Mg_{12}O_{12}$ -GlyGlyGly complexes.

configurations of the SCQDs, it seems that there are some exceptional cases. As an example, although we expect that both the HH_2 and the HH_1 configurations of $\text{Al}_2@C_{24}$ -GlyGlyGly and $\text{Al}_2@Mg_{12}O_{12}$ -GlyGlyGly should appear as subtractive, however, they appear to be additive. In other words, the results indicate that there might be some other intermolecular forces operating at the interfaces of such systems. Finally, some analysis from the energetic perspective maybe necessary in order to obtain a deeper insight.

Furthermore, considering the bar graph of Fig. 4 for $\text{Al}_2@C_{24}$ -GlyGlyGly cases, all the calculated values of $(P_{\text{complex}} - P_{\text{sumopt}})$ and $(P_{\text{complex}} - P_{\text{sumfrag}})$ are approximately the same, except for the HH_2 configuration wherein the difference between P_{sumopt} and P_{sumfrag} is significant. Equally, for $\text{Al}_2@Mg_{12}O_{12}$ -GlyGlyGly complexes, there is no significant

difference between the magnitude of the above-mentioned parameters, however, for the HT_1 case, there is a significant change of orientation of $(P_{\text{complex}} - P_{\text{sumopt}})$ relative to $(P_{\text{complex}} - P_{\text{sumfrag}})$ leading to their dipole moments change from 0.42D to -0.43D respectively. As a final point, it should be reiterated that this change of sign from positive to negative could be due to the appearance of density deformation phenomena.

3.2. Keesom energy and total electronic energy calculations

Fig. 5 displays both the calculated Keesom energy (KE) and the total electronic energy (TE) for the systems considered in this study. The KE energy represents the classical dipole-dipole interaction energy, and the total electronic energy provides the quantum interaction energy. Consequently, from Fig. 5 one can observe that the KE energy of both $\text{Al}_2@C_{24}$ and $\text{Al}_2@Mg_{12}O_{12}$

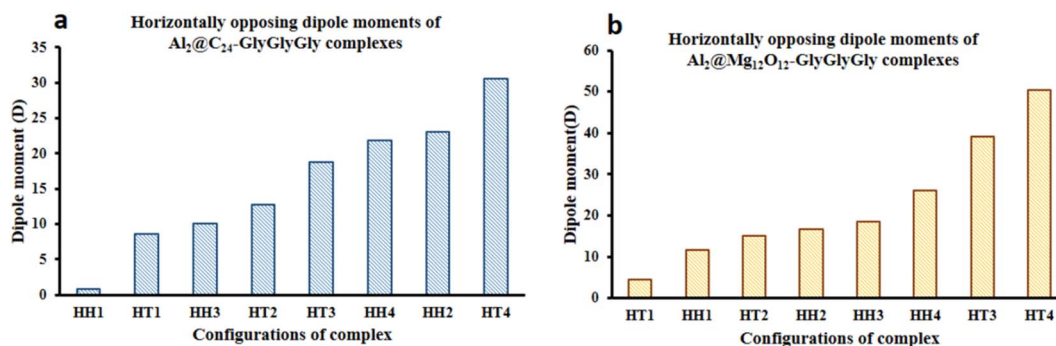


Fig. 3 Variations of the magnitude of the dipole moments with configuration (a) for $\text{Al}_2@C_{24}$ -GlyGlyGly and (b) for $\text{Al}_2@Mg_{12}O_{12}$ -GlyGlyGly.



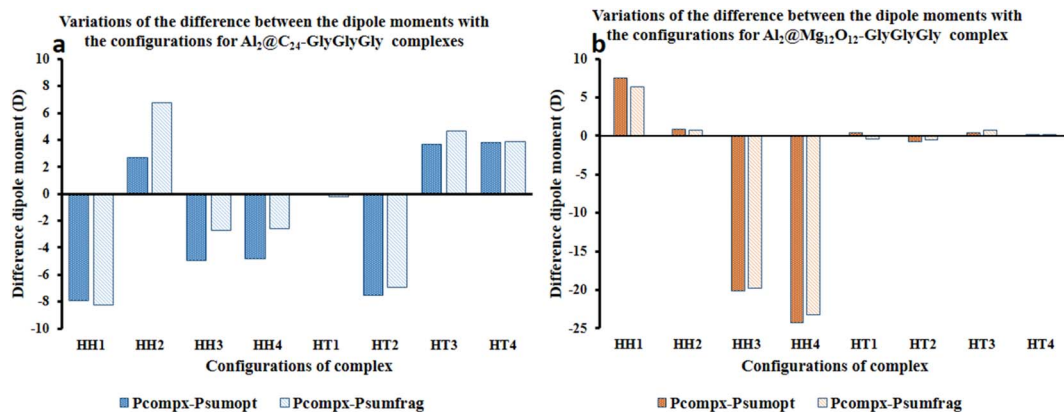


Fig. 4 Variations of the differences of the dipole moments for $(P_{\text{comp}} - P_{\text{sumopt}})$ and $(P_{\text{comp}} - P_{\text{sumfrag}})$ related to (a) $\text{Al}_2@C_{24}\text{-GlyGlyGly}$ and (b) $\text{Al}_2@Mg_{12}O_{12}\text{-GlyGlyGly}$ complexes when they are horizontally in opposite or the same orientations.

SCQDs coupled to GlyGlyGly tripeptides, for the HH₄ and the HT₄ configurations, are most stable for the former, and least stable for the later. Additionally, Fig. 5 shows that all of the HH configurations for $\text{Al}_2@C_{24}\text{-GlyGlyGly}$ and $\text{Al}_2@Mg_{12}O_{12}\text{-GlyGlyGly}$ are the most stable complexes except for the HH₁ of $\text{Al}_2@Mg_{12}O_{12}\text{-GlyGlyGly}$.

From the quantum interaction energy point of view, as shown in Fig. 6, configurations such as (HT₃, HT₁) and (HH₃, HT₂) provide respectively the highest and the lowest pairs of values of the quantum interaction energy for $\text{Al}_2@C_{24}\text{-GlyGlyGly}$ and $\text{Al}_2@Mg_{12}O_{12}\text{-GlyGlyGly}$ complexes. Additionally, Fig. 6 shows that the TE energy for both organic and inorganic SCQDs conjugated with GlyGlyGly, a mixture of the HT and the HH configurations are located in the left segment of the figure (present the stable structures).

Finally, we should mention that in our computation of the KE, we employed some approximations, *vis-à-vis* both the distance (d) and the angles (θ and φ) between the dipole moments of the complexes in eqn (1). These approximations imply that the calculated Keesom interaction energy does not have the exact value that it should.

From Fig. 5 and 6 it can be seen that the majority of the HH configurations have the most negative values of the energy for both the dipole-dipole and quantum interaction energies, and

are hence located in the left segment of the figures that present the most stable structures. However, for the TE energy of $\text{Al}_2@C_{24}\text{-GlyGlyGly}$ SCQD the most stable configuration is of the HT type and not of the HH type. In contrast, all of the complexes with the most positive values of the quantum and dipole-dipole interaction energies, have the least stable structures. These are assigned to the HT type configurations of both $\text{Al}_2@C_{24}\text{-GlyGlyGly}$ and $\text{Al}_2@Mg_{12}O_{12}\text{-GlyGlyGly}$.

To summarize, our results from Fig. 5 and 6 show that the computed values of the KE and the TE energies for both $\text{Al}_2@C_{24}\text{-GlyGlyGly}$ and $\text{Al}_2@Mg_{12}O_{12}\text{-GlyGlyGly}$ do not follow the same trend. Hence, it should be emphasized that the dipole-dipole interaction does not make a dominant contribution to the intermolecular force at the interface of the SCQDs with the tripeptide GlyGlyGly. Therefore, we could assume that other intermolecular interactions are operative at the interface. To elucidate this point, further analyses that will be reported in the following sections, are necessary. Furthermore, to determine the correlations between the values of:

1. The KE energy and the quantum interaction energy,
2. Dipole moment with the TE energy,
3. $(P_{\text{comp}} - P_{\text{sumopt}})$ with the TE energy,
4. $(P_{\text{comp}} - P_{\text{sumfrag}})$ with the TE energy,

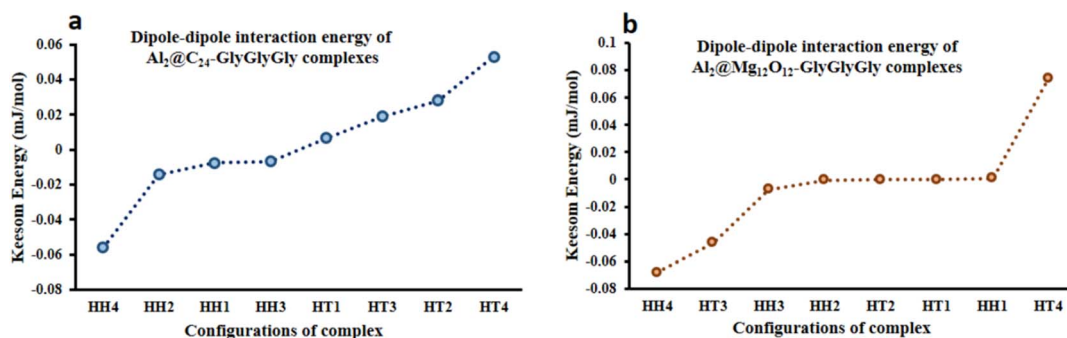


Fig. 5 Variations of the calculated Keesom energy with the configurations of the complexes; (a) $\text{Al}_2@C_{24}\text{-GlyGlyGly}$ and (b) $\text{Al}_2@Mg_{12}O_{12}\text{-GlyGlyGly}$.



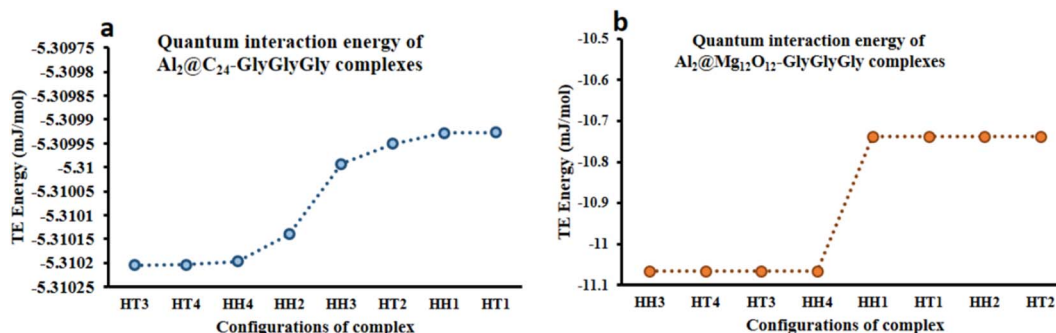


Fig. 6 Variations of the calculated total electronic interaction energy with the orientation of the complexes; (a) Al₂@C₂₄-GlyGlyGly and (b) Al₂@Mg₁₂O₁₂-GlyGlyGly.

we need to implement some specific statistical test to provide a quantitative relationship between all the calculated parameters. In the next section, these correlations are computed.

3.3. Calculated correlations

The statistical test is based on Pearson's correlation coefficient method⁶⁸ to determine whether any correlation exists between the parameters in the above 1–4 list. The results obtained for the coefficient of correlation (R) for cases (1, 2, 3, 4) are listed in Table 1. In this table, the positive values of R indicate that the changes in the correlated parameters for the cases (1, 2, 3, 4) follow the same trend, whereas the negative values indicate that the changes follow the opposite trend. Additionally, from the R^2 results in Table 1, we can state that the nearer these values are to 1, the stronger are the correlations and the nearer these values are to 0, the weaker are the correlations. Since the R^2 values, shown in Table 1, for cases 1–4 are small, therefore the correlations between the corresponding parameters are weak. Consequently, the results show that the dipole–dipole interactions are not the only contribution to the interaction energy of the systems studied, and that the contributions of other interaction energies are also significant. It should be mentioned that as far as the calculated energies are concerned, our results do not show the same trend *vis-à-vis* the classical and quantum interaction energies.

3.4. Analyses of electronic structures

3.4.1. Energy decomposition analysis. Energy decomposition analysis employs the Shubin Liu approach (EDA-SBL). We used this method to investigate the origin of the intermolecular

forces between the complexes. The results concerning the components of the EDA-SBL energy are shown in Fig. 7. From this figure we see that compared with the case Al₂@C₂₄-GlyGlyGly, the case Al₂@Mg₁₂O₁₂-GlyGlyGly has a rather larger interaction energy. Furthermore, the calculations reveal that the range of interaction energy is from -5.23753 to -11.0641 mJ mol⁻¹ for both Al₂@C₂₄-GlyGlyGly and Al₂@Mg₁₂O₁₂-GlyGlyGly complexes. The strongest interaction energy of Al₂@C₂₄ and Al₂@Mg₁₂O₁₂ with GlyGlyGly tripeptide belong to the HH₄ and the HT₃ cases with values of -5.23778 and -11.0641 mJ mol⁻¹ vdW respectively. Therefore, it is shown that unlike the Al₂@Mg₁₂O₁₂ SCQD, the HT configuration is the most stable orientation for the Al₂@C₂₄ SCQD. Finally, as for the contribution of intermolecular forces, it is obvious from Fig. 7 that the contribution of the electrostatic energy is dominant in all the selected complexes. However, both the steric and the quantum effects cannot be ignored for the current molecular systems.

Our calculations, therefore, reveal that there is a strong correlation, with $R^2 = 0.98$, for the eight selected complexes, half for Al₂@C₂₄ cases and half for Al₂@Mg₁₂O₁₂ cases as can be seen from Fig. 7. The values of components of E , *i.e.*, E_{elst} , E_{sterc} , E_{quantum} , are listed in Table 2. Moreover, Table 2 also shows the R -values of steric, electrostatic and quantum energies, and the total electronic energy of Al₂@C₂₄/Al₂@Mg₁₂O₁₂ SCQDs coupled to GlyGlyGly systems. According to these results, the relationship between the values of all the components and the total electronic energy is linear and is in the same direction when R is positive, and in the opposite direction when R is negative.

In order to reiterate the correlations between the interaction energy and the electrostatic, steric, and the quantum energies, from the energetic point of view, the calculated interaction energy either by the EDASBL method or with the M062X DFT method, shows a strong correlation with $R^2 = 0.98$ as seen in Table 2 for all of the eight selected complexes mentioned above. Finally, major contribution to the interaction energy of the selected cases is assigned to the electrostatic effect. However, we cannot completely associate this effect with the contribution of the dipole–dipole interaction energy; since, previous research⁶⁹ shows that the electrostatic energy, in addition to the dipole–dipole energy, consists of several other energies such as the dipole–quadrupole, the quadrupole–quadrupole energies *etc.*

Table 1 Calculated Pearson's correlation coefficient (R) and R^2 for demonstrating correlations between various calculated variables

Variables	R	R^2
KE energy and quantum interaction energy	0.1	0.01
Dipole moment with TE energy	-0.3	0.09
$(P_{\text{comp}} - P_{\text{sumopt}})$ with TE energy	0.2	0.04
$(P_{\text{comp}} - P_{\text{sumfrag}})$ with TE energy	0.3	0.09



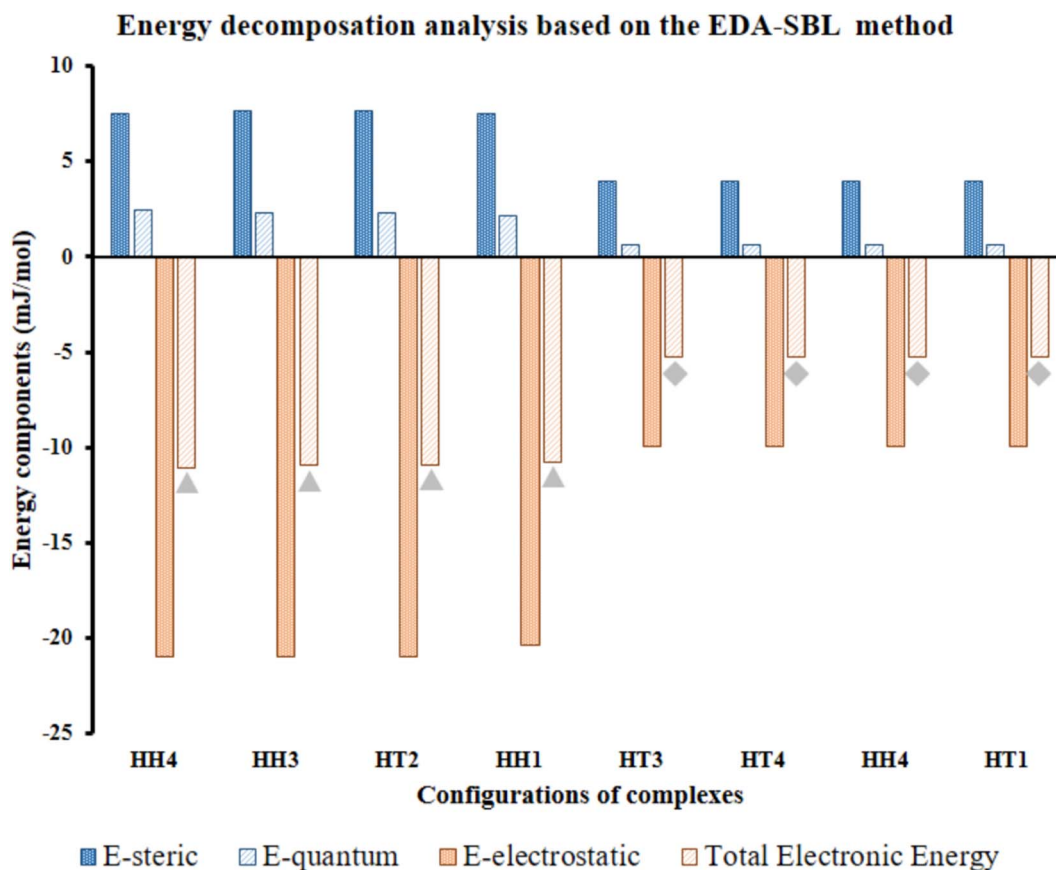


Fig. 7 Calculated EDA components of selected $\text{Al}_2@C_{24}$ -GlyGlyGly depicted by gray triangles and $\text{Al}_2@Mg_{12}O_{12}$ -GlyGlyGly shows by gray rhombuses according to the EDA-SBL method.

Table 2 Calculated Pearson's correlation coefficient (R) and R^2 for demonstrating correlations between various calculated energies

Variables	R	R^2
E_{steric} with TE	-0.99	0.98
E_{elst} with TE	0.99	0.98
E_{quantum} with TE	-0.99	0.98
TE energy from DFT with EDA	0.99	0.98

Therefore, performing specific analyses, like topological analysis, to ascertain the details of the nature of the intermolecular interactions are essential.

3.4.2. QTAIM analysis. Since interactions between $\text{Al}_2@C_{24}$ and $\text{Al}_2@Mg_{12}O_{12}$ SCQDs with GlyGlyGly tripeptide encompass several forms of both intermolecular and intramolecular interactions, therefore the QTAIM theory, as a powerful method, based on Bader's topological assumption,⁶⁴ is employed to investigate both the strength and nature of those interactions. Since, the QTAIM theory is employed, some topological parameters, such as the electron density $\rho(r)$, the Laplacian of the electron density $\nabla^2\rho(r)$, the electron energy density $H(r)$, which involves the potential $V(r)$, and the electron kinetic $G(r)$ energy density, are calculated at BCPs. Table 3 lists the values of these parameters. As can be observed from this table, the higher

the values of $\rho(r)$, the sharper the covalent character of the intermolecular forces is manifested. The highest values of the electron density are calculated to be 0.3 and 0.07 that belong to the HH₃ and the HT₃ configurations of $\text{Al}_2@Mg_{12}O_{12}$ and $\text{Al}_2@C_{24}$ complexes respectively.

We should mention that the combination of the signs of the electron energy density and the Laplacian of the electron density is imperative for determination of the nature of the intermolecular interaction. According to Rozas *et al.*,⁷⁰ the positive sign of $H(r)$ alone represents the shared interactions, while the negative sign exhibits the closed-shell interactions. Likewise, the negative values of $H(r)$ and $\nabla^2\rho(r)$ are strong manifestations of the covalent nature of interactions, whereas the positive values of $H(r)$ and $\nabla^2\rho(r)$ determine the weak electrostatic nature of interactions. However, if $H(r)$ has a negative sign and $\nabla^2\rho(r)$ has a positive sign, the dominant form of interaction is partially covalent in nature. For instance, from Table 3 it can be seen that between $\text{Al}_2@C_{24}$ and $\text{Al}_2@Mg_{12}O_{12}$ SCQDs with tripeptide, only $\text{Al}_2@Mg_{12}O_{12}$ -GlyGlyGly complexes that include the HH₃ and the HH₁ have negative values for both $H(r)$ and $\nabla^2\rho(r)$ topological parameters. Hence, we can attribute this to the sharing-interactions, such as the covalent bonding, which plays a significant role in the stability of the molecular systems.



Table 3 Results of electronic structure and topological analyses for optimized structures of both $\text{Al}_2\text{@C}_{24}$ and $\text{Al}_2\text{@Mg}_{12}\text{O}_{12}$ SCQDs with GlyGlyGly tripeptide

Complex	Configurations	BCPs	$\rho(r)$	$\nabla^2\rho(r)$	$V(r)$	$G(r)$	$H(r)$	$\frac{ V(r) }{G(r)}$	Ellipticity	$\frac{\lambda_1}{\lambda_3}$	ELF	LOL	sign $\lambda_2 \times \rho(r)$	
$\text{Al}_2\text{@Mg}_{12}\text{O}_{12}$ -GlyGlyGly	HH ₃	Mg-O...H...N	0.311	-1.737	-0.510	0.075	-0.585	7.75	0.001	1.09	0.97	0.84	-0.31	
		O-Mg...O	0.045	0.369	0.015	0.077	-0.063	0.81	0.020	0.14	0.04	0.18	-0.05	
		Al-O...H-O	0.331	-1.956	-0.561	0.072	-0.632	8.83	0.005	1.14	0.98	0.86	-0.33	
	HT ₂	Mg-O...H	0.022	0.061	-0.001	0.016	-0.018	1.07	0.039	0.22	0.09	0.23	-0.02	
		HH ₄	O...H...N	0.027	0.077	0.043	0.021	0.022	1.064	0.020	0.225	0.098	0.248	-0.03
	HH ₁	O-Al...H	0.005	0.008	0.000	0.002	-0.002	0.910	0.428	0.193	0.115	0.217	0.00	
		O...H-N	0.025	0.072	-0.001	0.019	-0.021	1.068	0.032	0.225	0.093	0.243	-0.03	
		Mg-O...C	0.045	0.348	0.013	0.074	-0.061	0.822	0.020	0.143	0.046	0.180	-0.04	
	$\text{Al}_2\text{@C}_{24}$ -GlyGlyGly	HT ₃	O...H-O	0.325	-1.888	-0.544	0.072	-0.616	8.538	0.002	1.131	0.974	0.860	-0.33
			C-C...H	0.012	0.035	0.001	0.008	-0.007	0.85	0.329	0.19	0.05	0.18	-0.01
			C-Al...O	0.074	0.596	0.011	0.139	-0.128	0.92	0.028	0.15	0.07	0.21	-0.07
		HT ₄	C-C...N	0.008	0.022	0.001	0.005	-0.004	0.79	1.146	0.20	0.04	0.17	-0.01
C-C...O			0.073	0.583	0.011	0.135	-0.124	0.92	0.013	0.15	0.07	0.21	-0.07	
HH ₄			C-Al...N	0.064	0.352	-0.002	0.090	-0.092	1.02	0.013	0.18	0.10	0.25	-0.06
HT ₁		C-C...N	0.006	0.016	0.000	0.004	-0.003	0.92	0.839	0.10	0.02	0.13	-0.01	
		C-C...H	0.015	0.041	0.001	0.010	-0.009	0.94	0.091	0.21	0.07	0.21	-0.01	
		Al-C...H	0.011	0.031	0.001	0.007	-0.006	0.88	0.810	0.19	0.05	0.19	-0.01	
		C-C...N	0.008	0.023	0.001	0.005	-0.005	0.88	0.253	0.15	0.03	0.16	-0.01	
		Al-C...H	0.004	0.013	0.001	0.003	-0.002	0.72	0.651	0.14	0.02	0.11	-0.004	
		Al-C...O	0.006	0.018	0.001	0.004	-0.003	0.85	0.550	0.14	0.02	0.13	-0.01	

From another perspective, the nature of the intermolecular forces can arise due to the balance that is established between the potential energy and the electron kinetic energy density at BCPs. Accordingly, the ratio $|V(r)|/G(r)$ must be calculated in order to demonstrate the nature of the intermolecular interactions,⁷⁰ since, when the value of this ratio is more than 2, the interaction is characterized as a covalent bond, and when it is between 1 and 2, the interaction is of mixed type, and finally when it is less than 1, it represents either a hydrogen bond (H-bond) or a vdW type of interaction. Table 3 shows that for the majority of the intermolecular interactions between GlyGlyGly and organic SCQDs, the ratio is less than 1, except for the HH₄ configuration of $\text{Al}_2\text{@C}_{24}$ -GlyGlyGly complex. By addressing this issue, the results show the dominance of the weak interactions such as the vdW or the H-bond for $\text{Al}_2\text{@C}_{24}$ -GlyGlyGly case. However, for the GlyGlyGly case and inorganic SCQDs, as shown in Table 3, the calculated values for the ratio involve all of the possible values, *i.e.*, less than 1, between 1 and 2, and greater than 2. For the inorganic SCQDs case, a range of interactions, from the weak to mixed and covalent, can be present.

From another aspect, the character of the intermolecular forces can be determined by the ratio $|\lambda_1/\lambda_3|$, where λ_3 presents the third largest Hessian matrix of eigenvalues, which serves as another AIM index.⁷¹ Therefore, when $|\lambda_1/\lambda_3|$ is less than 1 and $\nabla^2\rho(r)$ is greater than 0, this character is known as the outflow of $\rho(r)$ that can represent the closed-shell interactions such as the highly-polarized bond, the ionic bond, the vdW bond as well as the H-bond. In contrast, if $\nabla^2\rho(r)$ is less than 0 and $|\lambda_1/\lambda_3|$ is greater than 1, then the compression of $\rho(r)$ becomes significant and can be taken into account as the shared interactions representing the covalent bond.^{71,72} Since all of the complexes have positive values of the Laplacian, and $|\lambda_1/\lambda_3|$ is less than 1, we can infer that the closed-shell interactions like the vdW and the

hydrogen bond, and the high polarity bond play vital role *vis-à-vis* all of the selected cases except the HH₃ configurations of $\text{Al}_2\text{@Mg}_{12}\text{O}_{12}$ -GlyGlyGly complex.

According to the QTAIM analyses, shown in Table 3, it can be deduced that among the selected complexes, the majority of structures have positive values of $H(r)$ and the Laplacian, and $|\lambda_1/\lambda_3| < 1$. These values indicate that closed-shell interactions (the H-bond and the vdW) exist between the tripeptide and SCQDs. On the contrary, the minority of selected complexes, such as the HH₃ and the HH₁ configurations of $\text{Al}_2\text{@Mg}_{12}\text{O}_{12}$ -GlyGlyGly complexes, acquire negative values for $H(r)$, the Laplacian as well as the ratio $|\lambda_1/\lambda_3| > 1$ which demonstrate covalent bonding as the shared interaction types. Finally, the selected cases, like the HH₃ and the HH₁ configurations belonging to $\text{Al}_2\text{@Mg}_{12}\text{O}_{12}$ -GlyGlyGly complexes, can be categorized as strong interactions with electron density values of more than 0.3 au and the ellipticity index approaching 0, while for the rest of the structures, the values of the electron density are less than 0.1 that indicate weak interactions.

Apart from the above indices, the ellipticity ($\varepsilon = (\lambda_1/\lambda_2) - 1$), where λ_1 and λ_2 present the first and the second largest Hessian matrix of eigenvalues respectively, is introduced in the AIM theory⁷³ as an index to measure the deviation of $\rho(r)$ from the cylindrical symmetry. Table 3 shows that the HH₃ and the HT₄ have the ellipticity of 0.001 and 1.146 for $\text{Al}_2\text{@Mg}_{12}\text{O}_{12}$ -GlyGlyGly and $\text{Al}_2\text{@C}_{24}$ -GlyGlyGly *i.e.*, the lowest and the highest values respectively. Additionally, to further illustrate this point, one can state that there is a relationship between the ellipticity and the nature of the intermolecular interactions for both SCQDs coupled to GlyGlyGly and surrounded by water as the solvent. Whenever the shared interaction and the strong interaction are dominant in the HH₃ and the HH₁ configurations, the values of ε approach 0. Nevertheless, for the rest of the



complexes *i.e.*, $\text{Al}_2@C_{24}\text{-GlyGlyGly}$ or $\text{Al}_2@Mg_{12}O_{12}\text{-GlyGlyGly}$ that have closed-shell interactions, the values of ε deviate from 0 which imply a deviation from the cylindrical symmetry, and this can be attributed to a decrease in the π component of the bond.

3.4.3. Electron localization function and localized orbital locator. The ELF, and the LOL concepts were proposed by Becke and Edgecombe,⁷⁴ Schmider and Becke⁷⁵ respectively. We have applied these methods to further investigate the origin of the chemical bond within the system of SCQDs and GlyGlyGly tripeptide. The ELF always measures the electron localization and/or delocalization between 0 to 1, where 0 corresponds to complete delocalization and 1 to complete localization. Similarly, the LOL characterizes the nature of the bonding related to the $G(r)$ contributions that reveal the locations of the localized electrons without requiring the localized orbitals. The results are listed numerically in Table 3 and are shown graphically in Fig. 8. According to this table the computed values for the ELF are in the range of 0.01 au to 0.98 au, and the LOL values are in the range 0.10 au to 0.86 au for all the selected configurations of $\text{Al}_2@C_{24}\text{-GlyGlyGly}$ and $\text{Al}_2@Mg_{12}O_{12}\text{-GlyGlyGly}$ complexes. Furthermore, the calculated values of the ELF and the LOL for $\text{Al}_2@C_{24}\text{-GlyGlyGly}$ are less than 0.1 au and 0.3 au respectively, whereas for $\text{Al}@Mg_{12}O_{12}\text{-GlyGlyGly}$ system a variety of values could be observed from Table 3. For instance, the HH_3 and the HH_1 configurations have values of the ELF around 1 au and 0.9 au calculated as their LOL values.

Evidently, in accordance with Fig. 8, which depicts the map of the ELF and the LOL for the selected complexes, such as the HH_3 , the HH_1 and the HT_2 configurations for $\text{Al}_2@Mg_{12}O_{12}\text{-GlyGlyGly}$, the nature of the intermolecular interactions is computed to be covalent, partially-covalent-partially-electrostatic, and purely electrostatic respectively. While for the HH_4 , the HT_3 , and the HT_1 configurations of $\text{Al}_2@C_{24}\text{-GlyGlyGly}$, the nature of the intermolecular interactions is computed to be partially-covalent-partially-electrostatic and purely electrostatic respectively. It has been shown by Becke *et al.*⁷⁴ that the low (high) ELF values are attributed to fast (slow) electrons, and that the slow electrons serve as localized electrons like lone pairs and covalent bonds respectively. For this

reason, the higher the values of the LOL and the ELF, the greater is the electron density. Similar points also apply to the LOL.

3.4.4. NCI&RDG analyses. The NCI approach⁷⁶ together with the RDG (as an effective tool for depicting the NCI outputs graphically based on the RDG scatter plots) play significant roles concerning the real-space analysis for exploring the nature of weak interactions. We have performed the analyses to investigate and determine the possible type of noncovalent interactions that exist between the SCQDs and the tripeptide. The isosurfaces for the NCI maps of the selected complexes are displayed in Fig. 9. As can be seen from this figure the three colors, *i.e.*, red, green and blue regions, demonstrate the steric interactions (strong repulsion), the vdW (strong repulsion), and the strong hydrogen bond respectively. Furthermore, the NCI graphs are drawn with the sign of $(\lambda_2) \times \rho(r)$, wherein λ_2 is the horizontal axis, and the RDG scatter is the vertical axis. If the sign of $(\lambda_2) \times \rho(r)$ is positive then a repulsive interaction is detected, while attractive interaction is considered when this value is negative. Lastly, as can be seen from the table, all the signs of the computed values of $(\lambda_2) \times \rho(r)$ are negative for all of the selected configurations of $\text{Al}_2@C_{24}\text{-GlyGlyGly}$ and $\text{Al}_2@Mg_{12}O_{12}\text{-GlyGlyGly}$ complexes. Consequently, the total intermolecular forces, which exist between the tripeptide and the SCQDs, can be demonstrated to be attractive interactions (weak or strong). This point requires further analysis to be performed, in the same way as the RDG analysis, to provide an insight into this issue.

In the RDG scatter plots, shown in Fig. 9, there are various regions as well as colors such as blue, green and red with specific interpretation. Firstly, the data with positive values (spikes in the range of 0.1 to 0.5 au) indicate repulsive steric interactions. The next region, located around 0, relates to the vdW interactions. Finally, the weak attractive interactions appear in the negative zone of this plot. As a result, the values displayed by the RDG plots of the selected $\text{Al}_2@C_{24}\text{-GlyGlyGly}$ and $\text{Al}_2@Mg_{12}O_{12}\text{-GlyGlyGly}$ complexes, and given in Table 3, all correspond to the negative sign of $(\lambda_2) \times \rho(r)$. In addition, it should be emphasized that the negative values less than 0.1 au can be attributed to noncovalent interactions, such as those that appear for all of the $\text{Al}_2@C_{24}\text{-GlyGlyGly}$ complexes, while

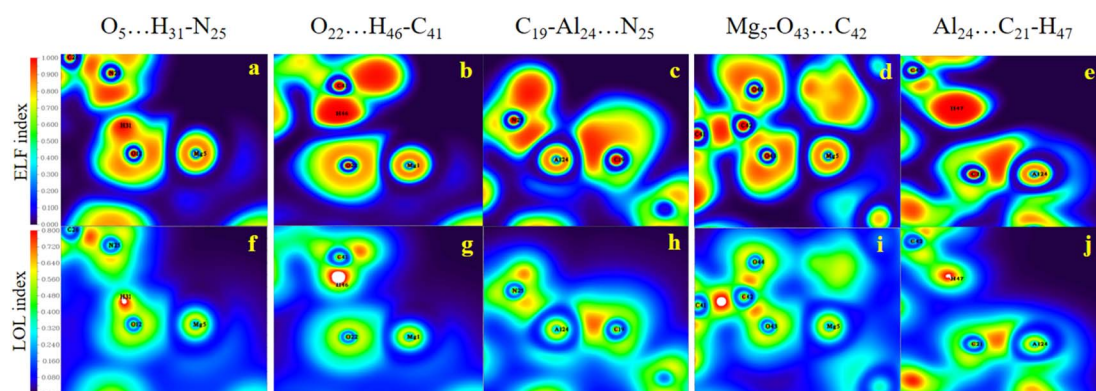


Fig. 8 The color-filled map of the ELF (a–e) and the LOL (f–j) of selected samples of $\text{Al}_2@C_{24}/\text{Mg}_{12}\text{O}_{12}$ SCQDs conjugated with GlyGlyGly (a) shared interactions (b) partially-covalent-partially electrostatic (c) pure electrostatic.

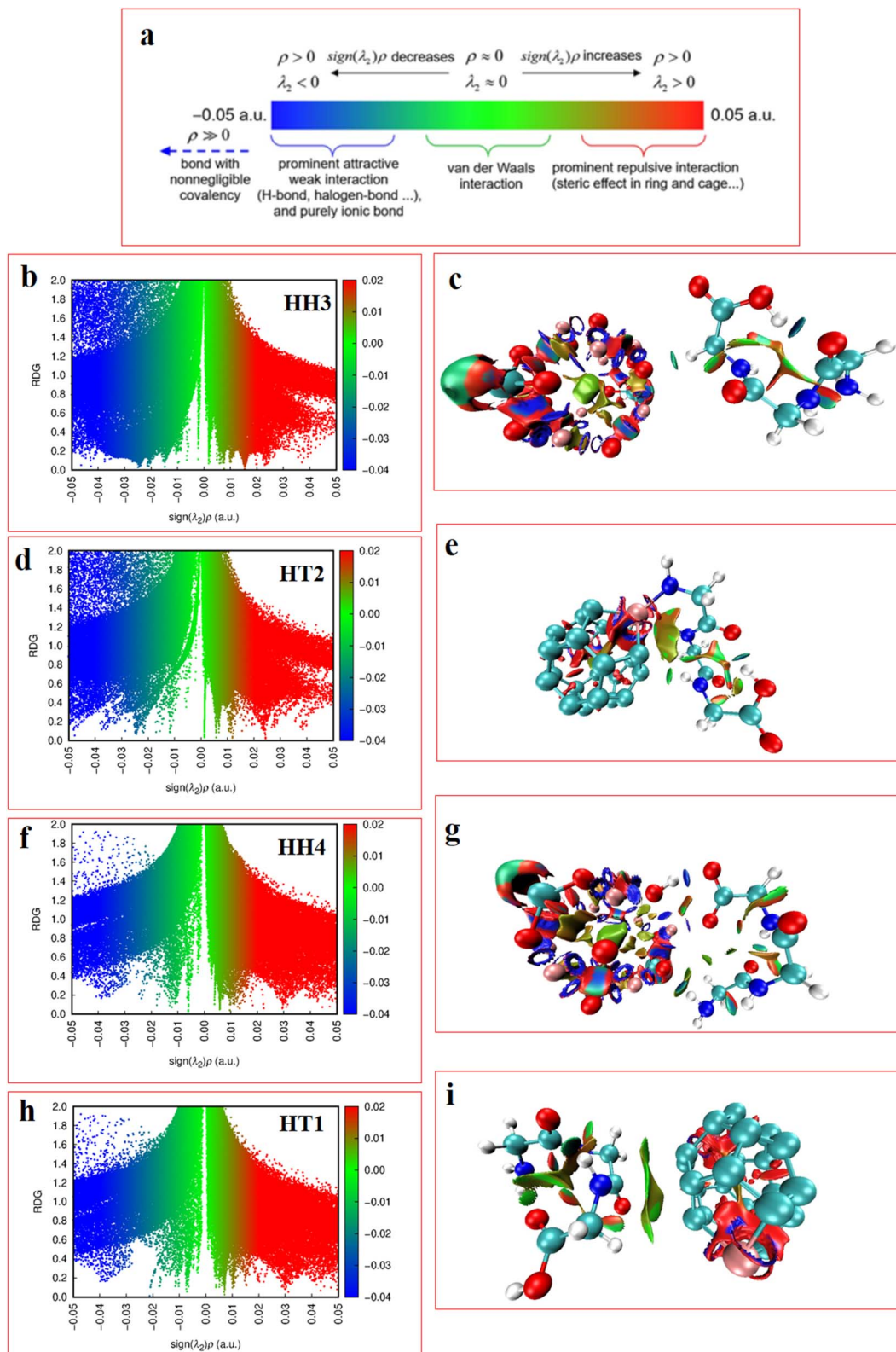


Fig. 9 Results of the NCI analyses (a) NCI and RDG indices, (b) and (c) RDG scatter plots (the right images) and the NCI counterpart visualized (the left cartoon images) concerning the HH₃; (d) and (e) the HT₂ of Al₂@Mg₁₂O₁₂-GlyGlyGly; (f), (g), (h), and (i) the HH₄ and the HT₁ configurations of Al₂@C₂₄-GlyGlyGly.



for some of the $\text{Al}_2\text{@Mg}_{12}\text{O}_{12}$ -GlyGlyGly cases the values are more than -0.1 au that are indicative of covalent interactions. Finally, in the NCI analyses shown in Fig. 9, both the green and yellow patches that appear between GlyGlyGly and the SCQDs represent the vdW interactions, whereas the red patches in the $\text{Al}_2\text{@C}_{24}$ and $\text{Al}_2\text{@Mg}_{12}\text{O}_{12}$ SCQDs depict the steric repulsion. Consequently, the vdW interactions, which are predominant interactions, compared to other intermolecular interactions, correspond to values in the range of -0.01 to 0.01 au on the RDG scatter plots. Ultimately, the small blue patches only emerge between the $\text{Al}_2\text{@Mg}_{12}\text{O}_{12}$ SCQDs with GlyGlyGly for the cases of the HH_3 and the HH_1 configurations as shown in the RDG isosurface.

4. Conclusion

In this paper, we investigated systematically the relationship between the magnitude and the direction of the electrical dipole moments and the interaction energy at the interfaces of the $\text{Al}_2\text{@C}_{24}$ -GlyGlyGly and $\text{Al}_2\text{@Mg}_{12}\text{O}_{12}$ -GlyGlyGly complexes. We employed the DFT method, based on the M062X and 6-31++G** as the level of the theory and the basis set respectively. It should be remarked that more sophisticated post-HF methods, such as the MPn and the QCI methods, provide higher accuracy than the general DFT-based methods. We also used the MP_2 method for some of the quantum dot systems. For example, we optimized the $\text{Al}_2\text{@Mg}_{12}\text{O}_{12}$ -GlyGlyGly complex at the $\text{MP}_2/6-31++\text{G}^{**}$ level using 32 processing cores (each having a clock rate of 2.6 GHz) and a total of 100 GB memory, with no frequency analysis. Under these conditions it took 2.5 real-time days (~ 85 days of CPU time) to perform the computations. Furthermore, there exists some benchmarking of the M062X method in the literature⁷⁷ that shows that this method provides reasonable results in comparison with the higher theoretical levels (such as the MP_n , etc.) and experimental observations. Our results also show that the values for the energy and the dipole moment obtained with the M062X method are close to those obtained from the MP_2 in units of Hartree and Debye, respectively as shown in Table 4.

Our calculated results of the dipole moments of the complexes indicate that there is no significant correlation between the values of the electrical dipole moments of complexes and their orientations. It should be pointed out that, according to the previously reported results, the combination of the dipole moments of selected complexes with the HT is of synergetic nature, and that of the HH is of an antagonistic nature. This is in contrast to the results that we have obtained;

namely an antagonistic behavior for the HT and synergetic behavior for the HH. This is due to the fact that in previous research only the pure electrostatic interactions were taken into account, whereas in addition to electrostatic interactions we have also considered the quantum and steric interactions.

We have calculated both the Keesom and the total electronic interaction energies wherein the dipole-dipole and the quantum interaction energies are present. Furthermore, the Pearson correlation coefficient test reveals that the correlations between the classical interaction energy and the quantum energy ($R^2 = 0.01$) as well as the variation in the difference of the dipole moments with the total electronic energy (with R^2 equal to 0.03 and 0.01) are categorized as the weak correlation type. The EDA analysis, based on the SBU scheme, demonstrates that for all the selected complexes, the electrostatic effect has a significant role, but the quantum and steric effects also play important roles at the interfaces of molecular systems. All the three approaches, the QTAIM, the ELF and the LOL, to a large extent reveal the nature of the intermolecular interactions. Likewise, the NCI-RDG analyses confirm the above-mentioned findings and reveal that the dipole-dipole interactions at the surfaces of the molecular systems play an important role in the intermolecular interactions. However, there are other types of intermolecular forces such as the vdW, the H-bond and the polarization attraction that can have decisive contributions to the interaction energy of the complexes.

Our molecular modeling can be helpful to provide an insight into the nature of the intermolecular forces. Consequently, one approach to obtain these forces is *via* the DFT method due to its lower computational cost and acceptable accuracy in comparison with the MP_2 method. As far as justification for the use of GlyGlyGly is concerned, it should be mentioned that since the limitations of the use of the quantum dots in clinical researches are related to their solvation capacity, therefore some biomolecules, like GlyGlyGly tripeptide, can play a significant role for overcoming these limitations. Finally, some tripeptides, like GlyGlyGly, can make contribution as a targeting agent in nano drug delivery vehicles.

Conflicts of interest

There are no conflicts to declare.

Acknowledgements

This paper has been extracted from the PhD thesis in the field of computational nanomedicine by Mr Hadi Mohammadi at the Department of Medical Physics and Biomedical Engineering in the School of Medicine, Shahid Beheshti University of Medical Sciences (Registration No: IR.SBMU.MSP.REC.1398.666). The authors gratefully acknowledge the help of Dr Reza Karbalaei for providing computing facilities and computer script codes checking.

References

- 1 D. Luo, C. Yan and T. Wang, *Small*, 2015, **11**, 5984–6008.

Table 4 Comparison between both the energy and the dipole moment calculated for $\text{Al}_2\text{@Mg}_{12}\text{O}_{12}$ -GlyGlyGly by M062X and MP_2 methods

	M062X	MP_2	Difference (%)
$\text{Al}_2\text{@Mg}_{12}\text{O}_{12}$ (energy)	-3514.14	-3297.96	6.6%
$\text{Mg}_{12}\text{O}_{12}$ -GlyGlyGly (dipole moment)	39.08	45.32	13.7%



- 2 Y. Sun, *Chem. Soc. Rev.*, 2013, **42**, 2497–2511.
- 3 K. J. M. Bishop, C. E. Wilmer, S. Soh and B. A. Grzybowski, *Small*, 2009, **5**, 1600–1630.
- 4 T. Wang, D. LaMontagne, J. Lynch, J. Zhuang and Y. C. Cao, *Chem. Soc. Rev.*, 2013, **42**, 2804–2823.
- 5 B. Abécassis, M. D. Tessier, P. Davidson and B. Dubertret, *Nano Lett.*, 2014, **14**, 710–715.
- 6 K. Pahnke, O. Altintas, F. G. Schmidt and C. Barner-Kowollik, *ACS Macro Lett.*, 2015, **4**, 774–777.
- 7 A. Sikder, S. Chakraborty, P. Rajdev, P. Dey and S. Ghosh, *Acc. Chem. Res.*, 2021, **54**, 2670–2682.
- 8 I. Insua, J. Bergueiro, A. Méndez-Ardoy, I. Lostalé-Seijo and J. Montenegro, *Chem. Sci.*, 2022, **13**, 3057–3068.
- 9 G. Chen and M. Jiang, *Chem. Soc. Rev.*, 2011, **40**, 2254–2266.
- 10 J. N. Israelachvili, *Intermolecular and surface forces*, Academic press, 2011.
- 11 P. H. Maccallum, R. Poet and E. J. Milner-White, *J. Mol. Biol.*, 1995, **248**, 361–373.
- 12 D. M. Smith and K. A. Woerpel, *Org. Biomol. Chem.*, 2006, **4**, 1195–1201.
- 13 A. Warshel, *Acc. Chem. Res.*, 1981, **14**, 284–290.
- 14 Y. L. Jiang, Y. Ichikawa, F. Song and J. T. Stivers, *Biochemistry*, 2003, **42**, 1922–1929.
- 15 L. D. Williams and L. J. Maher III, *Annu. Rev. Biophys. Biomol. Struct.*, 2000, **29**, 497–521.
- 16 J. A. Olsen, D. W. Banner, P. Seiler, U. Obst Sander, A. D'Arcy, M. Stihle, K. Müller and F. Diederich, *Angew. Chem., Int. Ed.*, 2003, **42**, 2507–2511.
- 17 I. Doytchinova, *Molecules*, 2022, **27**, 1496.
- 18 P. Politzer and J. S. Murray, *Chemical Reactivity in Confined Systems: Theory and Applications*, 2021, pp. 113–134.
- 19 J. S. Murray and P. Politzer, *Wiley Interdiscip. Rev.: Comput. Mol. Sci.*, 2017, **7**, e1326.
- 20 L. Schaeffer, in *The practice of medicinal chemistry*, Elsevier, 2008, pp. 464–480.
- 21 S. Shah, N. Rangaraj, S. B. Singh and S. Srivastava, *Colloid Interface Sci. Commun.*, 2021, **42**, 100406.
- 22 M. K. Mazumder, R. A. Sims, A. S. Biris, P. K. Srirama, D. Saini, C. U. Yurteri, S. Trigwell, S. De and R. Sharma, *Chem. Eng. Sci.*, 2006, **61**, 2192–2211.
- 23 A. Shurki, M. Strajbl, C. N. Schutz and A. Warshel, *Methods Enzymol.*, 2004, **380**, 52–84.
- 24 Y. Wang, R. Cai and C. Chen, *Acc. Chem. Res.*, 2019, **52**, 1507–1518.
- 25 S. T. Johnston, M. Faria and E. J. Crampin, *Nanoscale Adv.*, 2021, **3**, 2139–2156.
- 26 L. Abarca-Cabrera, P. Fraga-García and S. Berensmeier, *Biomater. Res.*, 2021, **25**, 1–18.
- 27 J. Li, N. Lu, S. Han, X. Li, M. Wang, M. Cai, Z. Tang and M. Zhang, *ACS Appl. Mater. Interfaces*, 2021, **13**, 21040–21050.
- 28 A. Hu, W. Zhang, G. Liao, D. Wang and Y. Peng, *Environ. Sci.: Nano*, 2020, **7**, 2795–2808.
- 29 I. Rouse, D. Power, E. G. Brandt, M. Schneemilch, K. Kotsis, N. Quirke, A. P. Lyubartsev and V. Lobaskin, *Phys. Chem. Chem. Phys.*, 2021, **23**, 13473–13482.
- 30 J. Subbotina and V. Lobaskin, *J. Phys. Chem. B*, 2022, **126**, 1301–1314.
- 31 V. Forest, M. Cottier and J. Pourchez, *Nano Today*, 2015, **10**, 677–680.
- 32 A. E. Nel, L. Mädler, D. Velegol, T. Xia, E. Hoek, P. Somasundaran, F. Klaessig, V. Castranova and M. Thompson, *Nat. Mater.*, 2009, **8**, 543–557.
- 33 G. Hu, B. Jiao, X. Shi, R. P. Valle, Q. Fan and Y. Y. Zuo, *ACS Nano*, 2013, **7**, 10525–10533.
- 34 E. Silla, A. Arnau and I. Tuñón, *Handbook Solvents*, 2001, vol. 7.
- 35 J. E. Schoutens, *J. Biol. Phys.*, 2005, **31**, 35–55.
- 36 S. J. Ganesan and S. Matysiak, *J. Chem. Theory Comput.*, 2014, **10**, 2569–2576.
- 37 E. J. Lien, Z.-R. Guo, R.-L. Li and C.-T. Su, *J. Pharm. Sci.*, 1982, **71**, 641–655.
- 38 H. Vovusha, R. G. Amorim, R. H. Scheicher and B. Sanyal, *RSC Adv.*, 2018, **8**, 6527–6531.
- 39 A. Das, A. Das and B. K. Banik, *J. Indian Chem. Soc.*, 2021, **98**, 100005.
- 40 A. Das and B. K. Banik, in *Green Approaches in Medicinal Chemistry for Sustainable Drug Design*, Elsevier, 2020, pp. 921–964.
- 41 S. Riahi, S. Eynollahi, M. R. Ganjali and P. Norouzi, *Int. J. Electrochem. Sci.*, 2010, **5**, 815–827.
- 42 J. C. Slater, *Phys. Rev.*, 1929, **34**, 1293.
- 43 E. U. Condon, *Phys. Rev.*, 1930, **36**, 1121.
- 44 C. Möller and M. S. Plesset, *Phys. Rev.*, 1934, **46**, 618.
- 45 B. Gidwani, V. Sahu, S. S. Shukla, R. Pandey, V. Joshi, V. K. Jain and A. Vyas, *J. Drug Deliv. Sci. Technol.*, 2021, **61**, 102308.
- 46 S. O. Souza, R. B. Lira, C. R. A. Cunha, B. S. Santos, A. Fontes and G. Pereira, *Top. Curr. Chem.*, 2021, **379**, 1–32.
- 47 Y. Fu, M.-S. Jang, T. Wu, J. H. Lee, Y. Li, D. S. Lee and H. Y. Yang, *Carbohydr. Polym.*, 2019, **224**, 115174.
- 48 A. M. Wagner, J. M. Knipe, G. Orive and N. A. Peppas, *Acta Biomater.*, 2019, **94**, 44–63.
- 49 E. Campbell, M. T. Hasan, R. Gonzalez Rodriguez, G. R. Akkaraju and A. V. Naumov, *ACS Biomater. Sci. Eng.*, 2019, **5**, 4671–4682.
- 50 M. J. Frisch, G. W. Trucks, H. B. Schlegel, G. E. Scuseria, M. A. Robb, J. R. Cheeseman, G. Scalmani, V. Barone, G. A. Petersson, H. Nakatsuji, X. Li, M. Caricato, A. V. Marenich, J. Bloino, B. G. Janesko, R. Gomperts, B. Mennucci, H. P. Hratchian, J. V. Ortiz, A. F. Izmaylov, J. L. Sonnenberg, D. Williams-Young, F. Ding, F. Lipparini, F. Egidi, J. Goings, B. Peng, A. Petrone, T. Henderson, D. Ranasinghe, V. G. Zakrzewski, J. Gao, N. Rega, G. Zheng, W. Liang, M. Hada, M. Ehara, K. Toyota, R. Fukuda, J. Hasegawa, M. Ishida, T. Nakajima, Y. Honda, O. Kitao, H. Nakai, T. Vreven, K. Throssell, J. A. Montgomery, Jr, J. E. Peralta, F. Ogliaro, M. J. Bearpark, J. J. Heyd, E. N. Brothers, K. N. Kudin, V. N. Staroverov, T. A. Keith, R. Kobayashi, J. Normand, K. Raghavachari, A. P. Rendell, J. C. Burant, S. S. Iyengar, J. Tomasi, M. Cossi, J. M. Millam, M. Klene, C. Adamo, R. Cammi, J. W. Ochterski, R. L. Martin, K. Morokuma,



- O. Farkas, J. B. Foresman and D. J. Fox, *Gaussian 16, Revision C.01*, Gaussian, Inc., Wallingford CT, 2016, <http://gaussian.com/citation/>.
- 51 R. Dennington, T. A. Keith, and J. M. Millam, *GaussView, Version 6.1*, Semichem Inc., Shawnee Mission, KS, 2016, <http://gaussian.com/citation/>.
- 52 V. Barone and M. Cossi, *J. Phys. Chem. A*, 1998, **102**, 1995–2001.
- 53 M. Cossi, N. Rega, G. Scalmani and V. Barone, *J. Comput. Chem.*, 2003, **24**, 669–681.
- 54 H. Ghafur Rauf, S. Majedi, E. Abdulkareem Mahmood and M. Sofi, *Chem. Rev. Lett.*, 2019, **2**, 140–150.
- 55 I. Ravaei, M. Haghighat and S. M. Azami, *Appl. Surf. Sci.*, 2019, **469**, 103–112.
- 56 Y. Cao, A. Khan, H. Balakheyli, A. N. K. Lup, M. R. Taghartapeh, H. Mirzaei, S. R. Khandoozi, A. Soltani, M. Aghaei and F. Heidari, *Arabian J. Chem.*, 2021, **14**, 103200.
- 57 M. Sheikhi, Y. Ahmadi, S. Kaviani and S. Shahab, *Struct. Chem.*, 2021, **32**, 1181–1196.
- 58 Y. Gao, F. Xu, J. Wu, H. Zhao and A. G. Ebadi, *Comput. Theor. Chem.*, 2022, **1207**, 113507.
- 59 B. L. Ndjopme Wandji, A. D. Tamafo Fouegue, N. K. Nkungli, R. A. Ntieche and A. Wahabou, *R. Soc. Open Sci.*, 2022, **9**, 211650.
- 60 A. S. Rad, V. Samipour, S. Movaghgharnezhad, A. Mirabi, M. H. Shahavi and B. K. Moghadas, *Surf. Interfaces*, 2019, **15**, 30–37.
- 61 S. Liu, *J. Chem. Phys.*, 2007, **126**, 244103.
- 62 K. F. Biegler, J. Schnbohm and D. Bayles, *J. Comput. Chem.*, 2001, **22**(5), 545–559.
- 63 T. Lu and F. Chen, *J. Comput. Chem.*, 2012, **33**, 580–592.
- 64 R. F. W. Bader, *Acc. Chem. Res.*, 1985, **18**, 9–15.
- 65 P. Wu, R. Chaudret, X. Hu and W. Yang, *J. Chem. Theory Comput.*, 2013, **9**, 2226–2234.
- 66 W. Humphrey, A. Dalke and K. Schulten, *J. Mol. Graph.*, 1996, **14**, 33–38.
- 67 T. Williams and C. Kelley, *Gnuplot 4.5: an interactive plotting program.*, 2011, <http://gnuplot.info>.
- 68 A. L. Edwards, *Correl. Coeff.*, 1976, 33–46.
- 69 A. Volkov and P. Coppens, *J. Comput. Chem.*, 2004, **25**, 921–934.
- 70 I. Rozas, I. Alkorta and J. Elguero, *J. Am. Chem. Soc.*, 2000, **122**, 11154–11161.
- 71 R. F. W. Bader and H. Essén, *J. Chem. Phys.*, 1984, **80**, 1943–1960.
- 72 D. Cremer and E. Kraka, *Croat. Chem. Acta*, 1984, **57**, 1259.
- 73 R. F. W. Bader, T. S. Slee, D. Cremer and E. Kraka, *J. Am. Chem. Soc.*, 1983, **105**, 5061–5068.
- 74 A. D. Becke and K. E. Edgecombe, *J. Chem. Phys.*, 1990, **92**, 5397–5403.
- 75 H. L. Schmider and A. D. Becke, *J. Mol. Struct.: THEOCHEM*, 2000, **527**, 51–61.
- 76 A. Otero-De-La-Roza, E. R. Johnson and J. Contreras-García, *Phys. Chem. Chem. Phys.*, 2012, **14**, 12165–12172.
- 77 A. L. Hickey and C. N. Rowley, *J. Phys. Chem. A*, 2014, **118**, 3678–3687.

